

TOPOLOGICAL TIME SERIES ANALYSIS

JOSE A. PEREA

ABSTRACT. Time series are ubiquitous in our data rich world. In what follows I will describe how ideas from dynamical systems and topological data analysis can be combined to gain insights from time-varying data. We will see several applications to the live sciences and engineering, as well as some of the theoretical underpinnings.

1. LORENZ AND THE BUTTERFLY

Imagine you have a project involving a crucial computer simulation. For an initial value $\mathbf{v}_0 = (x_0, y_0, z_0) \in \mathbb{R}^3$, a sequence $\mathbf{v}_0, \dots, \mathbf{v}_n \in \mathbb{R}^3$ is computed in such a way that \mathbf{v}_{j+1} is determined from \mathbf{v}_j for $j = 0, \dots, n - 1$. After the simulation is complete you realize that a rerun is needed for further analysis. Instead of initializing at \mathbf{v}_0 , which might take a while, you take a shortcut: you input a value \mathbf{v}_j selected from the middle of the current results, and the simulation runs from there while you go for coffee. Figure 1 is displayed on the computer monitor upon your return; the orange curve is the sequence x_0, \dots, x_n from the initial simulation, and the blue curve is the x coordinate for the rerun initialized at \mathbf{v}_j :

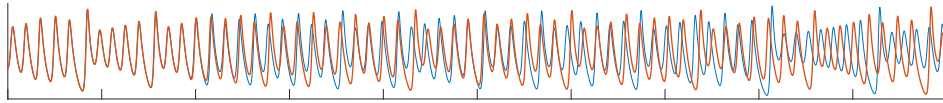


FIGURE 1. Orange: results from the simulation initialized at \mathbf{v}_0 ;
blue: results after manually restarting the simulation from \mathbf{v}_j .

The results agree at first, but then they diverge widely; what is going on? Edward Norton Lorenz, a mathematical meteorologist, asked himself the very same question while studying a simplified model (1) for weather forecasting [18]. In the process of resolving the aforementioned discrepancy, which one could erroneously attribute to software error or a hardware malfunction, Lorenz laid out the foundations for what we know today as chaos theory. The relevant set of differential equations for the simplified model, called the Lorenz system, is shown in equation (1); x, y and

2010 *Mathematics Subject Classification*. Primary 55R99, 55N99, 68W05; Secondary 55U99.

Key words and phrases. Time series analysis, Dynamical systems, Sliding window embeddings, Persistent homology.

This work was partially supported by the NSF under grant DMS-1622301 and DARPA under grant HR0011-16-2-003.

z are real-valued functions of time t , and $\sigma, \rho, \beta \in \mathbb{R}$ are physical constants.

$$\begin{aligned} x'(t) &= \sigma \cdot (y - x) \\ y'(t) &= x \cdot (\rho - z) - y \\ z'(t) &= xy - \beta z \end{aligned} \tag{1}$$

Solving the Lorenz system yields a differentiable function

$$\Phi : \mathbb{R} \times \mathbb{R}^3 \longrightarrow \mathbb{R}^3 \tag{2}$$

where $\Phi(t, \mathbf{v}_0) = (x(t), y(t), z(t))$ satisfies (1) for all $t \in \mathbb{R}$, and $\Phi(0, \mathbf{v}_0) = \mathbf{v}_0$ for all $\mathbf{v}_0 \in \mathbb{R}^3$. In fact, the orange curve from Figure 1 corresponds to $\Phi(t, (5, 5, 5))$ when $(\sigma, \rho, \beta) = (10, 28, 8/3)$. The discrepancy between the orange and blue curves, as elucidated in [18], is a property inherent to the system. Lorenz realized that when manually entering \mathbf{v}_j as input, he only used the first few significant digits instead of the full precision values. In other words, the system (1) can be extremely sensitive to initial conditions in that any errors are compounded exponentially with time.

This behavior is known today as the *Butterfly Effect*. The metaphor is that even the tiniest change in initial atmospheric conditions, e.g. such as a butterfly flapping its wings in Brazil, may change the long-term evolution of weather patterns enough to produce a tornado in Texas. Such unpredictability is one of the hallmarks of a *chaotic dynamical system*, and speaks to the futility of long-term weather prediction. The butterfly metaphor is further amplified by the shape of the solution $t \mapsto \Phi(t, (5, 5, 5)) = (x(t), y(t), z(t))$, $0 \leq t \leq 200$, shown in Figure 2 (left).

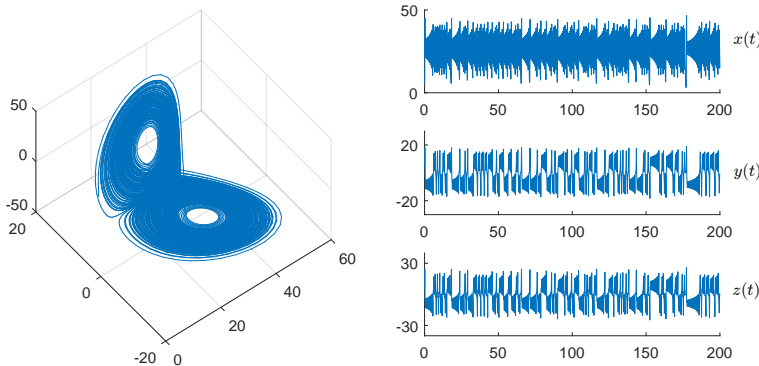


FIGURE 2. Lorenz's butterfly attractor

Dynamical systems are mathematical abstractions of time-dependent physical processes. Intuitively speaking, a dynamical system consists of two pieces of data: a set of states M — e.g., all possible atmospheric conditions at a given location on earth — along with rules $\Phi = \{\Phi_p : p \in M\}$ describing how each state $p \in M$ changes over time. More specifically,

Definition 1.1. A global continuous time dynamical system is a pair (M, Φ) , where M is a topological space and $\Phi : \mathbb{R} \times M \longrightarrow M$ is a continuous map so that $\Phi(0, p) = p$, and $\Phi(s, \Phi(t, p)) = \Phi(s + t, p)$ for all $p \in M$ and all $t, s \in \mathbb{R}$.

The typical examples arising from differential equations (e.g., the Lorenz system) have as state space a smooth manifold M (e.g., \mathbb{R}^3), and the dynamics are given by the integral curves (e.g., equation (2)) of a smooth vector field on M (e.g., (1)).

Some subsets of M are specially important since they attract the evolution of states in close proximity. Indeed, a set $A \subset M$ is called an attractor if it satisfies three conditions: (1) it is compact, (2) it is an invariant set — that is, if $a \in A$ then $\Phi(t, a) \in A$ for all $t \geq 0$ — and (3) it has an open basin of attraction. In other words, there is an invariant open neighborhood $U \subset M$ of A , so that

$$\bigcap_{t \geq 0} \{\Phi(t, p) : p \in U\} = A$$

An attractor is called strange — and this is just a name — if it exhibits fractal properties. For instance, Lorenz’s butterfly $\Lambda \subset \mathbb{R}^3$ from Figure 2 is one of the most widely known examples of a strange attractor.

2. PERSISTENT HOMOLOGY: MEASURING SHAPE FROM FINITE SAMPLES

The shape of attractors carries a great deal of information about the global structure of a dynamical system. Indeed, attractors with the shape of a circle $S^1 = \{z \in \mathbb{C} : |z| = 1\}$ give rise to periodic processes; fractal geometry is evidence of chaotic behavior; while high-dimensional tori $\mathbb{T}^n = S^1 \times \dots \times S^1$ are linked to quasiperiodicity. The latter is a type of recurrence emerging from the superposition of periodic oscillators with *incommensurate* (i.e., linearly independent over \mathbb{Q}) frequencies. Quasiperiodicity appears, for example, in turbulent fluids [25], and the detection of biphonation in high-speed laryngeal videoendoscopy [29] — i.e., videos of vibrating vocal folds. Similarly, the existence of chaos in brain activity is a question of considerable interest in neuroscience [16], as is the presence of periodic oscillators in biological systems [26].

A data analysis question that has received significant attention in recent years is how to measure the shape of a topological space \mathbb{X} — e.g., an attractor — from a finite set X (the data) approximating it. This is the type of problem driving advances in Topological Data Analysis [6], and where tools like persistent homology [21] — which we will describe next — are relevant. If M is a metric space with metric ρ , and $\mathbb{X}, X \subset M$, then the quality of the approximation of \mathbb{X} by X can be quantified as follows. For $\alpha \in \mathbb{R}$, define the α -offset of $Z \subset M$ as

$$Z^{(\alpha)} = \left\{ y \in M : \inf_{z \in Z} \rho(y, z) \leq \alpha \right\} \tag{3}$$

and the *Hausdorff distance* between Z and \tilde{Z} as

$$d_H(Z, \tilde{Z}) := \inf \left\{ \alpha > 0 : Z \subset \tilde{Z}^{(\alpha)} \text{ and } \tilde{Z} \subset Z^{(\alpha)} \right\} \tag{4}$$

The typical strategy in topological data analysis is to replace the finite sample X by a space whose shape captures that of \mathbb{X} , provided $d_H(X, \mathbb{X})$ is small enough. Indeed, for $Z \subset M$ and $\alpha \in \mathbb{R}$, the *Rips complex* of Z at scale α is the set

$$R_\alpha(Z) := \left\{ \{z_0, \dots, z_k\} \subset Z : \rho(z_i, z_j) \leq \alpha \text{ for all } 0 \leq i, j \leq k \right\} \tag{5}$$

This is in fact a *simplicial complex*; points in Z can be thought of as vertices, sets with two elements $\{z_0, z_1\} \in R_\alpha(Z)$ are edges, $\{z_0, z_1, z_2\} \in R_\alpha(Z)$ is a triangular face, and so on. A theorem of Janko Latschev [17] contends that if \mathbb{X} is a closed

Riemannian manifold and $d_H(X, \mathbb{X})$ is small, X not necessarily finite, then (the geometric realization of) $R_\alpha(X)$ is homotopy equivalent to \mathbb{X} for small α .

The homotopy type of a space refers to those properties which are invariant under continuous deformations; e.g., is it connected? are there holes? and they can be quantified using *singular homology*. Given an integer $n \geq 0$, the n -th homology of a topological space B with coefficients in a field \mathbb{F} is a vector space $H_n(B; \mathbb{F})$. Its dimension $\beta_n(B; \mathbb{F})$ — the n -th *Betti number* of B with coefficients in \mathbb{F} — provides a count for the number of essentially distinct n -dimensional holes in B . Indeed, if $\mathbb{F} = \mathbb{Q}$, then $\beta_0(B) = \beta_0(B; \mathbb{Q})$ counts the number of path-connected components of B , $\beta_1(B)$ is the number of essentially distinct loops in B bounding a hole, $\beta_2(B)$ is roughly the number of closed 2-dimensional regions bounding a void, and so on for $n \geq 3$. Here is an example: the 2-dimensional torus $\mathbb{T}^2 = S^1 \times S^1$ in Figure 3 (left) has Betti numbers $\beta_0(\mathbb{T}^2) = 1$ since it is path-connected, $\beta_1(\mathbb{T}^2) = 2$ since it has a horizontal and a vertical hole, $\beta_2(\mathbb{T}^2) = 1$ since \mathbb{T}^2 encloses an empty volume, and $\beta_n(\mathbb{T}^2) = 0$ for all $n \geq 3$. Similarly, the 2-sphere $S^2 = \{\mathbf{x} \in \mathbb{R}^3 : \|\mathbf{x}\| = 1\}$ has Betti numbers $\beta_0(S^2) = \beta_2(S^2) = 1$, $\beta_1(S^2) = 0$, and $\beta_n(S^2) = 0$ for $n \geq 3$.

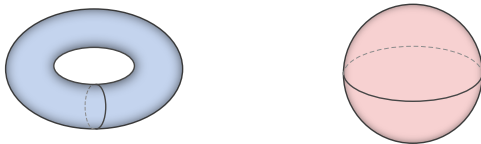


FIGURE 3. Left: The 2-dimensional torus $\mathbb{T}^2 = S^1 \times S^1$. Right: The 2-sphere $S^2 = \{\mathbf{x} \in \mathbb{R}^3 : \|\mathbf{x}\| = 1\}$.

Continuous maps $f : B \rightarrow B'$ between topological spaces can also be studied through the lens of homology. Indeed, any such f induces linear transformations $f_n : H_n(B; \mathbb{F}) \rightarrow H_n(B'; \mathbb{F})$, $n \geq 0$, between the corresponding homology vector spaces in such a way that if $id : B \rightarrow B$ is the identity of B , then id_n is the identity of $H_n(B; \mathbb{F})$, and $(f \circ g)_n = f_n \circ g_n$ whenever compositions make sense.

For realistic data $X \subset M$, the Betti numbers $\alpha \mapsto \beta_n(R_\alpha(X); \mathbb{F})$ are expected to be fairly unstable as α varies. Indeed, sampling artifacts or noise in X can produce holes which are present in $R_\alpha(X)$ but not in $R_{\alpha+\delta}(X)$ for small $\delta > 0$ (e.g., see Figure 4 below). This is where comparing the homology of spaces related by maps is useful. Indeed, let $\mathcal{Z} = \{Z_\alpha\}_{\alpha \in \mathbb{R}}$ be a family of spaces such that $Z_\alpha \subset Z_{\alpha'}$ for all pairs $\alpha \leq \alpha'$. Such a family is called a *filtration*, and we have already seen two examples: The offset filtration $\{Z^{(\alpha)}\}_{\alpha \in \mathbb{R}}$ defined in equation (3), and the Rips filtration $\mathcal{R}(Z) = \{R_\alpha(Z)\}_{\alpha \in \mathbb{R}}$ from (5). Given a filtration $\mathcal{Z} = \{Z_\alpha\}_{\alpha \in \mathbb{R}}$ and $\alpha \leq \alpha'$, the inclusion map $\iota^{\alpha, \alpha'} : Z_\alpha \hookrightarrow Z_{\alpha'}$ induces linear transformations

$$\iota_n^{\alpha, \alpha'} : H_n(Z_\alpha; \mathbb{F}) \rightarrow H_n(Z_{\alpha'}; \mathbb{F}) \quad , \quad n \geq 0 \quad (6)$$

Classes in $H_n(Z_\alpha; \mathbb{F})$ which are not in the Kernel of $\iota_n^{\alpha, \alpha'}$ for large $\alpha' - \alpha$, are interpreted as being persistent throughout the filtration. The collection of vector spaces and linear maps resulting from (6) is called the n -dimensional *persistent homology*, with coefficients in \mathbb{F} , of the filtration \mathcal{Z} . More generally,

Definition 2.1. A persistence vector space \mathbf{V} is a collection of vector spaces V_α , $\alpha \in \mathbb{R}$, and linear transformations $\iota^{\alpha, \alpha'} : V_\alpha \rightarrow V_{\alpha'}$, $\alpha \leq \alpha'$, so that:

- (1) $\iota^{\alpha, \alpha}$ is the identity of V_α for every $\alpha \in \mathbb{R}$.

$$(2) \iota^{\alpha', \alpha''} \circ \iota^{\alpha, \alpha'} = \iota^{\alpha, \alpha''}, \text{ whenever } \alpha \leq \alpha' \leq \alpha''.$$

Two persistence vector spaces $\mathbf{V} = \{V_\alpha, \iota^{\alpha, \alpha'}\}$ and $\mathbf{W} = \{W_\alpha, \kappa^{\alpha, \alpha'}\}$ are isomorphic, denoted $\mathbf{V} \cong \mathbf{W}$, if there are linear isomorphisms $T_\alpha : V_\alpha \rightarrow W_\alpha$ for all $\alpha \in \mathbb{R}$, so that $\kappa^{\alpha, \alpha'} \circ T_\alpha = T_{\alpha'} \circ \iota^{\alpha, \alpha'}$ whenever $\alpha \leq \alpha'$.

We will concentrate on three quantities for a nonzero element $\gamma \in V_\alpha$:

$$\begin{aligned} \text{birth}(\gamma) &:= \inf \left\{ \tilde{\alpha} \leq \alpha : \gamma \in \text{Image} \left(\iota^{\tilde{\alpha}, \alpha} \right) \right\} \\ \text{death}(\gamma) &:= \sup \left\{ \alpha' \geq \alpha : \gamma \notin \text{Kernel} \left(\iota^{\alpha, \alpha'} \right) \right\} \\ \text{persistence}(\gamma) &:= \text{death}(\gamma) - \text{birth}(\gamma) \end{aligned} \quad (7)$$

As we saw before, the Betti numbers capture the homology of a space and hence yield a succinct shape descriptor for its topology. Persistent homology, on the other hand, describes the evolution of homological features in a filtration. Under favorable circumstances [8] it can be described by an invariant called *the barcode*:

Theorem 2.2. *Let $\mathbf{V} = \{V_\alpha, \iota^{\alpha, \alpha'}\}$ be a persistence vector space so that $\dim(V_\alpha)$ is finite for all $\alpha \in \mathbb{R}$. Then, there exists a multiset (i.e., a set whose elements may appear with repetitions) of intervals $I \subset [-\infty, \infty]$ called the barcode of \mathbf{V} , and denoted $\text{bcd}(\mathbf{V})$, so that:*

- (1) *It subsumes the Betti numbers: If $\alpha \in \mathbb{R}$, then $\dim(V_\alpha)$ is exactly the number of intervals $I \in \text{bcd}(\mathbf{V})$, counted with repetitions, so that $\alpha \in I$.*
- (2) *It encodes persistence: For every $I \in \text{bcd}(\mathbf{V})$ and every $\alpha \in I$, there exists $\gamma \in V_\alpha$ so that the left and right end-points of I are $\text{birth}(\gamma)$ and $\text{death}(\gamma)$, respectively.*
- (3) *It is an invariant: If \mathbf{W} is a persistence vector space with $\dim(W_\alpha) < \infty$ for all $\alpha \in \mathbb{R}$, then $\text{bcd}(\mathbf{V}) = \text{bcd}(\mathbf{W})$ if and only if $\mathbf{V} \cong \mathbf{W}$.*

We will use $\text{bcd}_n^{\mathcal{R}}(X; \mathbb{F})$ to denote the barcode for the n -dimensional persistent homology of the Rips filtration on a metric space X . Below in Figure 4 we show an example for $X \subset \mathbb{R}^2$ sampled with noise around the unit circle S^1 , the Rips complex $R_\alpha(X)$ at $\alpha = 0, 0.36, 0.6, 1.21$, and the intervals (i.e., the horizontal blue lines) which comprise the barcode $\text{bcd}_1^{\mathcal{R}}(X; \mathbb{Z}/2)$. The computations were performed using the C++ library `Rips` [3]. The long interval is indicative of a persistent 1-dimensional hole in the data, which is consistent with X being sampled around S^1 ; recall that $\beta_1(S^1; \mathbb{Z}/2) = 1$. The short-lived intervals, on the other hand, are due to noise and sampling artifacts.

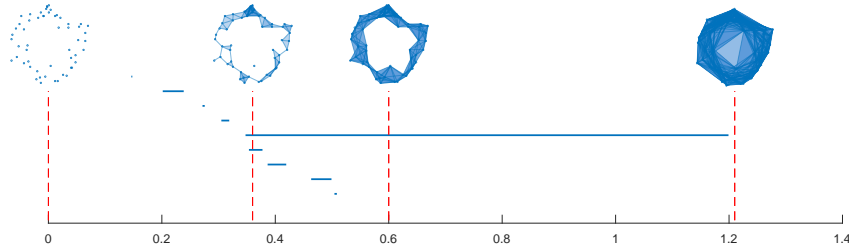


FIGURE 4. Barcode for the Rips filtration on $X \subset \mathbb{R}^2$ near S^1 .

As we have seen, persistent homology can be used to infer the topology of a space \mathbb{X} given a finite sample X : the number of long intervals in $\text{bcd}_n^{\mathcal{R}}(X; \mathbb{F})$ suggests a value for $\beta_n(\mathbb{X}; \mathbb{F})$. The barcodes $\text{bcd}_n^{\mathcal{R}}(X; \mathbb{F})$ can also be used to quantify/identify properties of dynamical systems: if \mathbb{X} is an attractor, a barcode like the one in Figure 4 would be indicative of periodicity, while the barcodes in Figure 5 would point to quasiperiodicity. Moreover, measures of fractal geometry can also be derived from persistent homology; see for instance [19] and [24].

3. ATTRACTOR RECONSTRUCTION: TIME SERIES DATA, TAKENS' THEOREM AND SLIDING WINDOW EMBEDDINGS

In practice it is exceedingly rare to have an explicit mathematical description of a dynamical system of interest. Instead, often times one can gather measurements of relevant quantities for each state $p \in M$ — e.g., in weather prediction one can estimate temperature, pressure, etc. A way of measuring can be thought of as a continuous map $F : M \rightarrow \mathbb{R}$ — called an *observation function* — and given an initial state $p \in M$, one obtains the time series

$$\begin{aligned} \varphi_p : \mathbb{R} &\longrightarrow \mathbb{R} \\ t &\longmapsto F \circ \Phi(t, p) \end{aligned} \quad (8)$$

For example, the blue and orange curves from Figure 1 are examples of time series from the Lorenz system. A single time series may appear to be a complete oversimplification of the underlying dynamics. The Takens' embedding theorem, due to Floris Takens [27], implies that they can actually be very useful:

Theorem 3.1. *Let M be a smooth, compact, Riemannian manifold; let $\tau > 0$ be a real number and let $d \geq 2 \dim(M)$ be an integer. If $\Phi \in C^2(\mathbb{R} \times M, M)$ and $F \in C^2(M, \mathbb{R})$ are generic, then for $\varphi_p(t)$ defined by (8), the delay map*

$$\begin{aligned} \varphi : M &\longrightarrow \mathbb{R}^{d+1} \\ p &\longmapsto (\varphi_p(0), \varphi_p(\tau), \varphi_p(2\tau), \dots, \varphi_p(d\tau)) \end{aligned} \quad (9)$$

is an embedding.

Here generic means that the set of functions Φ, F for which (9) is an embedding forms an open and dense set with respect to the Whitney topology. In fact, if $A \subset M$ is a strange attractor, then φ restricted to A will be (generically) an embedding whenever d is at least twice the box counting (a notion of fractal) dimension of A . Takens' theorem motivates the following definition,

Definition 3.2. Let $f : \mathbb{R} \rightarrow \mathbb{R}$ be a function, $\tau > 0$ a real number and $d > 0$ an integer. The *sliding window embedding* of f , with parameters d and τ , is the vector-valued function

$$\begin{aligned} SW_{d,\tau}f : \mathbb{R} &\longrightarrow \mathbb{R}^{d+1} \\ t &\longmapsto (f(t), f(t+\tau), f(t+2\tau), \dots, f(t+d\tau)) \end{aligned} \quad (10)$$

The integer $d+1$ is the dimension, τ is the delay and the product $d\tau$ is the window size. For $T \subset \mathbb{R}$, the set

$$SW_{d,\tau}f = \{SW_{d,\tau}f(t) : t \in T\} \quad (11)$$

is the *sliding window point cloud* associated to T .

Hence, given time series data $f(t) = \varphi_p(t)$ observed from a potentially unknown dynamical system (M, Φ) , Takens' theorem implies that (generically) the sliding window point cloud $\mathbb{S}\mathbb{W}_{d,\tau}f$ provides a topological copy of $\{\Phi(t, p) : t \in T\} \subset M$. In particular, this will reconstruct attractors. The underlying shape of $\mathbb{S}\mathbb{W}_{d,\tau}f$ can then be quantified with persistent homology, and the associated barcodes $\text{bcd}_n^{\mathcal{R}}(\mathbb{S}\mathbb{W}_{d,\tau}f; \mathbb{F})$ can be used as features in inference, classification, and learning tasks [12, 24, 30]. We will see shortly several applications of these ideas to science and engineering; for now, here is an instantiation of the pipeline:

Example. Let $\omega \in \mathbb{R}$ be irrational; we will use $\omega = \sqrt{3}$ for computations but any other choice would do. Consider the dynamics Φ and the observation function F on the torus $\mathbb{T}^2 = S^1 \times S^1 \subset \mathbb{C}^2$, given by

$$\begin{aligned} \Phi : \quad \mathbb{R} \times \mathbb{T}^2 &\longrightarrow \mathbb{T}^2 & F : \quad \mathbb{T}^2 &\longrightarrow \mathbb{R} \\ (t, (z_1, z_2)) &\mapsto (e^{it}z_1, e^{i\omega t}z_2) & (z_1, z_2) &\mapsto \text{Re}(z_1 + z_2) \end{aligned}$$

If $p \in \mathbb{T}^2$, then $\{\Phi(t, p) : t \in \mathbb{R}\}$ is dense in \mathbb{T}^2 , and hence \mathbb{T}^2 is the only attractor; e.g., see [5], page 86, Example 6.15. For $p = (1, 1)$ we obtain the quasiperiodic time series $f(t) = F \circ \Phi(t, (1, 1)) = \cos(t) + \cos(\omega t)$, and we show in Figure 5 the dynamics $t \mapsto \Phi(t, (1, 1))$ on the torus (left), the resulting time series $f(t)$ (center), and the barcodes $\text{bcd}_n = \text{bcd}_n^{\mathcal{R}}(\mathbb{S}\mathbb{W}_{d,\tau}f; \mathbb{Z}/2)$ in dimensions $n = 0, 1, 2$ (right).

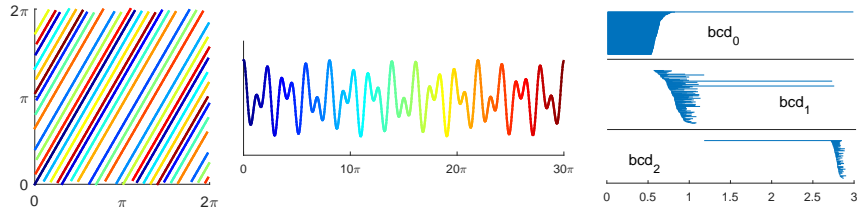


FIGURE 5. Left: The dynamics Φ on the torus. The colors, blue through red, indicate the time t for $t \mapsto \Phi(t, (1, 1)) \in \mathbb{T}^2$. Center: The time series $f(t) = F \circ \Phi(t, (1, 1)) = \cos(t) + \cos(\sqrt{3}t)$. The colors indicate the time variable $t \in [0, 30\pi]$ and are coordinated with the torus on the left panel. Right: Barcodes for the Rips filtration $\mathcal{R}(\mathbb{S}\mathbb{W}_{d,\tau}f)$; the number of long intervals recovers the Betti numbers of the attractor: $\beta_0(\mathbb{T}^2) = \beta_2(\mathbb{T}^2) = 1, \beta_1(\mathbb{T}^2) = 2$.

4. SOME APPLICATIONS OF SLIDING WINDOW PERSISTENCE

Wheeze Detection. A wheeze is an abnormal whistling sound produced while breathing. It is often associated with obstructed airways and lung diseases such as asthma, lung cancer and congestive heart failure. In [11], Emrani, Gentimis and Krim show that the 1-dimensional barcode $\text{bcd}_1^{\mathcal{R}}(\mathbb{S}\mathbb{W}_{d,\tau}f; \mathbb{F})$, and particularly the length of its longest interval (i.e., its maximum persistence)

$$\text{mp}_1^{\mathcal{R}}(\mathbb{S}\mathbb{W}_{d,\tau}f; \mathbb{F}) = \max \left\{ \text{length}(I) : I \in \text{bcd}_1^{\mathcal{R}}(\mathbb{S}\mathbb{W}_{d,\tau}f; \mathbb{F}) \right\} \quad (12)$$

is an effective feature for wheezing detection in recorded breathing sounds. Indeed, the presence of wheezing leads to circular sliding window point clouds. When

testing on a large database of sound recordings, Emrani et. al. shown that (12) leads to a higher detection accuracy than that of competing methods.

Periodicity Quantification in Gene Expression Data. Many biological processes, including the cell cycle, cell division, and the circadian clock, are periodic in nature. An important problem in systems biology is to describe these mechanisms at a genetic level [26]. Biologists approach this by first collecting data; specifically, how gene expression changes across time in a given model organism — e.g., yeast, mice, etc. Given said data, it is shown in [23] that measures similar to (12) can outperform state-of-the-art methods for periodicity quantification, and lead to the discovery of novel clock-regulated genes.

Segmentation of Dynamic Regimes. Complex high-dimensional systems can exhibit abrupt changes in qualitative behavior. For instance, the hearth’s climate has undergone several sudden transitions to and back from a “snowball earth” [13]. Identifying markedly different regimes in a system’s evolution can thus be used for warning, modeling and parameter estimation purposes [9]. Berwald et. al. show in [4] that, given time series data, effective classifiers can be trained on features from the barcodes of sliding window point clouds, with the goal of automatically segmenting a system into different behavioral regimes. Some applications of their methodology include the detection of bifurcations on stochastic and chaotic systems, as well as the analysis of temperature and CO₂ levels in ice cores.

Chatter Detection and Classification in Machining. Turning and milling are cutting processes used extensively in industrial manufacturing. Chatter, or machining vibrations, are wide oscillations of the cutting tool with respect to the metal workpiece; these undesired movements leave surface flaws on the production piece during turning and milling. Khasawneh et. al. show in [14, 15] that, given time series describing the undulations of the cutting piece, $\text{bcd}_1^{\mathcal{R}}(\text{SW}_{d,\tau}f; \mathbb{F})$ can be used as input features in classification algorithms for chatter detection.

Motion Recognition from Wearable Sensors. Dirafzoon et. al. show in [10] that barcodes on sliding window point clouds from motion capture time series, can be used to classify activities with very high accuracy.

Periodicity and Quasiperiodicity in Video Data. A video can be thought of as sampling a function $f : \mathbb{R} \rightarrow \mathbb{R}^k$. It follows that computing $\text{bcd}_n^{\mathcal{R}}(\text{SW}_{d,\tau}f; \mathbb{F})$ for the sliding window point $\text{SW}_{d,\tau}f \subset \mathbb{R}^{k(d+1)}$ can be used to detect recurrent behavior in video data, without the need for tracking or surrogate signals. See for instance [29] for applications of these ideas to the problem of quantifying periodicity and quasiperiodicity in video data, as well as the synthesis of slow-motion videos from recurrent movements [28].

5. THEORETICAL INVESTIGATIONS OF SLIDING WINDOW PERSISTENCE

The barcodes $\text{bcd}_n^{\mathcal{R}}(\text{SW}_{d,\tau}f; \mathbb{F})$ have been used successfully in several applications. However, very little is known about their theoretical behavior with respect to the parameters d, τ , the field \mathbb{F} and the homological dimension n . One of the main difficulties lies in that our knowledge of the homotopy type/homology of the Rips complex $R_\alpha(X)$, for arbitrary α , is rather limited: planar circles are essentially the

only spaces where we have complete answers [1]. I would like to highlight next some of what we do know.

Sliding Window Persistence of Periodic Functions. Let $\mathbb{T} = \mathbb{R}/2\pi\mathbb{Z}$ and let $C^1(\mathbb{T}, \mathbb{R})$ denote the set of continuously differentiable real-valued functions on \mathbb{T} . As a warm up example, let $\zeta(t) = \sin(Lt + \phi)$, for $L \in \mathbb{N}$ and $\phi \in \mathbb{R}$. A bit of trigonometry shows that

$$SW_{d,\tau}\zeta(t) = \sin(Lt + \phi)\mathbf{u} + \cos(Lt + \phi)\mathbf{v}$$

where $\mathbf{u} = SW_{d,\tau}\cos(Lt)|_{t=0}$ and $\mathbf{v} = SW_{d,\tau}\sin(Lt)|_{t=0}$. It readily follows that if $d \geq 1$ and the set $\{\mathbf{u}, \mathbf{v}\}$ is linearly independent, then $\mathbb{S}W_{d,\tau}\zeta = SW_{d,\tau}\zeta(\mathbb{T})$ is a planar ellipse. The semi-major and semi-minor axes can be computed explicitly as

$$a = \sqrt{\frac{(d+1) + \left| \frac{\sin(L(d+1)\tau)}{\sin(L\tau)} \right|}{2}} \quad \text{and} \quad b = \sqrt{\frac{(d+1) - \left| \frac{\sin(L(d+1)\tau)}{\sin(L\tau)} \right|}{2}} \quad (13)$$

The persistent homology of the Rips filtration on ellipses with small eccentricity, i.e. when $b < a < \sqrt{2}b$, has been recently studied by Adamaszek et. al. [2]. In particular, their work implies that if

$$\alpha_1 = \frac{4\sqrt{3}ab^2}{a^2 + 3b^2} \quad \text{and} \quad \alpha_2 = \frac{4\sqrt{3}a^2b}{3a^2 + b^2}$$

then the homotopy type of $R_\alpha(\mathbb{S}W_{d,\tau}\zeta)$ for $0 < \alpha \leq \alpha_2$ is either that of the circle, or that of a wedge of 2-dimensional spheres as follows:

$$R_\alpha(\mathbb{S}W_{d,\tau}\zeta) \simeq \begin{cases} S^1 & \text{for } 0 < \alpha < \alpha_1 \\ S^2 & \text{for } \alpha = \alpha_1 \\ \bigvee^5 S^2 & \text{for } \alpha_1 < \alpha < \alpha_2 \\ \bigvee^3 S^2 & \text{for } \alpha = \alpha_2 \end{cases}$$

The range $\alpha_1 < \alpha < \alpha_2$ is specially interesting since only one of the five 2-dimensional classes persists. In other words, the linear transformation

$$H_2(R_\alpha(\mathbb{S}W_{d,\tau}\zeta); \mathbb{F}) \longrightarrow H_2(R_{\alpha'}(\mathbb{S}W_{d,\tau}\zeta); \mathbb{F})$$

has rank one for every $\alpha_1 < \alpha < \alpha' < \alpha_2$. We readily obtain the following,

Theorem 5.1. *Let $\zeta(t) = \sin(Lt + \phi)$ for $L \in \mathbb{N}$, $\phi \in \mathbb{R}$, and for $d \in \mathbb{N}$, $\tau > 0$ let $a, b \geq 0$ be as in (13). If $a < \sqrt{2}b$ and \mathbb{F} is a field, then the maximum persistence (12) in dimensions 1 and 2 satisfies*

$$\begin{aligned} \text{mp}_1^{\mathcal{R}}(\mathbb{S}W_{d,\tau}\zeta; \mathbb{F}) &= \frac{4\sqrt{3}ab^2}{a^2 + 3b^2} \\ \text{mp}_2^{\mathcal{R}}(\mathbb{S}W_{d,\tau}\zeta; \mathbb{F}) &\geq \frac{4\sqrt{3}a^2b}{3a^2 + b^2} - \frac{4\sqrt{3}ab^2}{a^2 + 3b^2} \end{aligned}$$

The cases $\alpha > \alpha_2$ for $a < \sqrt{2}b$, and $\alpha > 0$ for $a \geq \sqrt{2}b$, are currently open. The case $a = b$, i.e. when $\mathbb{S}W_{d,\tau}\zeta$ is a circle, is much better understood. This happens when the window size $d\tau$ is equal to (an integer multiple of) $\frac{d}{d+1} \frac{2\pi}{L}$, which is a

little bit under $\text{Period}(\zeta) = \frac{2\pi}{L}$. Since the homotopy type of $R_\alpha(S^1)$ is known for all $\alpha > 0$ [1], we get that

$$R_\alpha(\text{SW}_{d,\tau}\zeta) \simeq \begin{cases} S^{2k+1} & \text{for } \sin\left(\frac{\pi k}{2k+1}\right) < \frac{\alpha}{\sqrt{2(d+1)}} < \sin\left(\frac{\pi(k+1)}{2k+3}\right) \\ \bigvee^{|\mathbb{R}|} S^{2k} & \text{for } \alpha = \sqrt{2(d+1)} \sin\left(\frac{\pi k}{2k+1}\right) \end{cases}$$

where the linear transformation

$$H_{2k+1}(R_\alpha(\text{SW}_{d,\tau}\zeta); \mathbb{F}) \longrightarrow H_{2k+1}(R_{\alpha'}(\text{SW}_{d,\tau}\zeta); \mathbb{F})$$

is an isomorphism (with rank one) for every

$$\sqrt{2(d+1)} \sin\left(\frac{\pi k}{2k+1}\right) < \alpha \leq \alpha' < \sqrt{2(d+1)} \sin\left(\frac{\pi(k+1)}{2k+3}\right).$$

Therefore,

Theorem 5.2. *Let $\zeta(t) = \sin(Lt + \phi)$, let \mathbb{F} be a field, and let $\tau = \frac{2\pi}{L(d+1)}$. Then, for every integer $k \geq 1$, $\text{mp}_{2k}^{\mathcal{R}}(\text{SW}_{d,\tau}\zeta; \mathbb{F}) = 0$ and*

$$\text{mp}_{2k-1}^{\mathcal{R}}(\text{SW}_{d,\tau}\zeta; \mathbb{F}) = \sqrt{2(d+1)} \cdot \left(\sin\left(\frac{\pi k}{2k+1}\right) - \sin\left(\frac{\pi(k-1)}{2k-1}\right) \right)$$

One strategy to understand $\text{dgm}_n^{\mathcal{R}}(\text{SW}_{d,\tau}f; \mathbb{F})$ for a general function $f \in C^1(\mathbb{T}, \mathbb{R})$, is to first approximate f by its truncated Fourier series

$$S_N f(t) = \sum_{|n| \leq N} \widehat{f}(n) e^{int} \quad , \quad \widehat{f}(n) = \frac{1}{2\pi} \int_{\mathbb{T}} f(t) e^{-int} dt$$

and then investigate the asymptotic behavior of the sequence of barcodes

$$\text{bcd}_n^{\mathcal{R}}(\text{SW}_{d,\tau} S_N f; \mathbb{F}) \quad , \quad N \in \mathbb{N} \tag{14}$$

Indeed, the analysis of $\zeta(t) = \sin(Lt + \phi)$ presented earlier can be bootstrapped to trigonometric polynomials, and the stability Theorem [7] can be used to study $\text{bcd}_n^{\mathcal{R}}(\text{SW}_{d,\tau}f; \mathbb{F})$ via the behavior of (14) as $N \rightarrow \infty$. This line of reasoning was explored in [22]. In particular, it results in sights for the choice of window size (it should be approximately $\frac{d}{d+1}$ times the period length), the embedding dimension (larger than twice the number of relevant harmonics) and the choice of field of coefficients (one whose characteristic does not divide $\frac{2\pi}{\text{Period}(f)}$). We end with a theorem [22, 6.8] relating the sliding window persistence of f to its harmonic content:

Theorem 5.3. *Let $f \in C^1(\mathbb{T}, \mathbb{R})$ be so that $f(t + \frac{2\pi}{L}) = f(t)$ for all $t \in \mathbb{T}$, and assume (for simplicity) that f has been centered and normalized:*

$$\widehat{f}(0) = 0 \quad , \quad \|f\|_2 := \left(\frac{1}{2\pi} \int_{\mathbb{T}} |f(t)|^2 dt \right)^{1/2} = 1$$

Let $\tau_d = \frac{2\pi}{L(d+1)}$, $T \subset \mathbb{T}$ and $\text{SW}_{d,\tau_d} f = \text{SW}_{d,\tau_d} f(T)$. If $f'(t) = \frac{df}{dt}$, then

$$\sup_{d \in \mathbb{N}} \text{mp}_1^{\mathcal{R}}(\text{SW}_{d,\tau_d} f; \mathbb{Q}) \geq 2\sqrt{3} \sup_{n \in \mathbb{Z}} |\widehat{f}(n)| - 2\sqrt{2} \|f'\|_2 d_H(T, \mathbb{T})$$

Beyond Periodicity. Very little is known about the sliding window persistence of other families of functions; there are a few results for quasiperiodic functions [20], but the rest of the landscape is essentially uncharted territory.

REFERENCES

- [1] M. Adamaszek and H. Adams. The vietoris–rips complexes of a circle. *Pacific Journal of Mathematics*, 290(1):1–40, 2017.
- [2] M. Adamaszek, H. Adams, and S. Reddy. On vietoris–rips complexes of ellipses. *Journal of Topology and Analysis*, pages 1–30.
- [3] U. Bauer. Ripser: a lean c++ code for the computation of vietoris-rips persistence barcodes. 2017. Software available at <https://github.com/Ripser/ripser>.
- [4] J. J. Berwald, M. Gidea, and M. Vejdemo-Johansson. Automatic recognition and tagging of topologically different regimes in dynamical systems. *Discontinuity, Nonlinearity, and Complexity*, 3(4):413–126, 2014.
- [5] W. M. Boothby. *An introduction to differentiable manifolds and Riemannian geometry*, volume 120. Academic press, 1986.
- [6] G. Carlsson. Topological pattern recognition for point cloud data. *Acta Numerica*, 23:289, 2014.
- [7] F. Chazal, D. Cohen-Steiner, M. Glisse, L. J. Guibas, and S. Y. Oudot. Proximity of persistence modules and their diagrams. In *Proceedings of the twenty-fifth annual symposium on Computational geometry*, pages 237–246. ACM, 2009.
- [8] W. Crawley-Boevey. Decomposition of pointwise finite-dimensional persistence modules. *Journal of Algebra and its Applications*, 14(05):1550066, 2015.
- [9] V. Dakos, M. Scheffer, E. H. van Nes, V. Brovkin, V. Petoukhov, and H. Held. Slowing down as an early warning signal for abrupt climate change. *Proceedings of the National Academy of Sciences*, 105(38):14308–14312, 2008.
- [10] A. Dirafzoon, N. Lokare, and E. Lobaton. Action classification from motion capture data using topological data analysis. In *Signal and Information Processing (GlobalSIP), 2016 IEEE Global Conference on*, pages 1260–1264. IEEE, 2016.
- [11] S. Emrani, T. Gentimis, and H. Krim. Persistent homology of delay embeddings and its application to wheeze detection. *IEEE Signal Processing Letters*, 21(4):459–463, 2014.
- [12] J. Garland, E. Bradley, and J. D. Meiss. Exploring the topology of dynamical reconstructions. *Physica D: Nonlinear Phenomena*, 334:49–59, 2016.
- [13] P. F. Hoffman, A. J. Kaufman, G. P. Halverson, and D. P. Schrag. A neoproterozoic snowball earth. *science*, 281(5381):1342–1346, 1998.
- [14] F. A. Khasawneh and E. Munch. Chatter detection in turning using persistent homology. *Mechanical Systems and Signal Processing*, 70:527–541, 2016.
- [15] F. A. Khasawneh, E. Munch, and J. A. Perea. Chatter classification in turning using machine learning and topological data analysis. In *14th IFAC Workshop on Time Delay Systems TDS 2018*, volume 51, pages 195–200. International Federation of Automatic Control, 2018.
- [16] H. Korn and P. Faure. Is there chaos in the brain? ii. experimental evidence and related models. *Comptes rendus biologiques*, 326(9):787–840, 2003.
- [17] J. Latschev. Vietoris-rips complexes of metric spaces near a closed riemannian manifold. *Archiv der Mathematik*, 77(6):522–528, 2001.
- [18] E. N. Lorenz. Deterministic nonperiodic flow. *Journal of the atmospheric sciences*, 20(2):130–141, 1963.
- [19] R. MacPherson and B. Schweinhart. Measuring shape with topology. *Journal of Mathematical Physics*, 53(7):073516, 2012.

- [20] J. A. Perea. Persistent homology of toroidal sliding window embeddings. In *2016 IEEE International Conference on Acoustics, Speech and Signal Processing (ICASSP)*, pages 6435–6439. IEEE, 2016.
- [21] J. A. Perea. A brief history of persistence. *preprint arXiv:1809.03624*, 2018. <https://arxiv.org/abs/1809.03624>.
- [22] J. A. Perea and J. Harer. Sliding windows and persistence: An application of topological methods to signal analysis. *Foundations of Computational Mathematics*, 15(3):799–838, 2015.
- [23] J. A. Perea, A. Deckard, S. B. Haase, and J. Harer. Sw1pers: Sliding windows and 1-persistence scoring; discovering periodicity in gene expression time series data. *BMC bioinformatics*, 16(1):257, 2015.
- [24] V. Robins. Towards computing homology from finite approximations. In *Topology proceedings*, volume 24, pages 503–532, 1999.
- [25] D. Ruelle and F. Takens. On the nature of turbulence. *Communications in mathematical physics*, 20(3):167–192, 1971.
- [26] G. Rustici, J. Mata, K. Kivinen, P. Lió, C. J. Penkett, G. Burns, J. Hayles, A. Brazma, P. Nurse, and J. Bähler. Periodic gene expression program of the fission yeast cell cycle. *Nature genetics*, 36(8):809, 2004.
- [27] F. Takens. Detecting strange attractors in turbulence. In *Dynamical systems and turbulence, Warwick 1980*, pages 366–381. Springer, 1981.
- [28] C. J. Tralie and M. Berger. Topological eulerian synthesis of slow motion periodic videos. In *2018 25th IEEE International Conference on Image Processing (ICIP)*, pages 3573–3577, 2018.
- [29] C. J. Tralie and J. A. Perea. (quasi) periodicity quantification in video data, using topology. *SIAM Journal on Imaging Sciences*, 11(2):1049–1077, 2018.
- [30] B. Xu, C. J. Tralie, A. Antia, M. Lin, and J. A. Perea. Twisty takens: A geometric characterization of good observations on dense trajectories. *arXiv preprint arXiv:1809.07131*. <https://arxiv.org/pdf/1809.07131>.

DEPARTMENT OF COMPUTATIONAL MATHEMATICS, SCIENCE & ENGINEERING
DEPARTMENT OF MATHEMATICS,
MICHIGAN STATE UNIVERSITY
EAST LANSING, MI, USA.
E-mail address: joperea@msu.edu